The Journal of Neuroscience, December 1, 2002, 22(23):10277–10290

Roles of Tetrodotoxin (TTX)-Sensitive Na^+ Current, TTX-Resistant Na^+ Current, and Ca^{2+} Current in the Action Potentials of Nociceptive Sensory Neurons

Nathaniel T. Blair and Bruce P. Bean

Department of Neurobiology, Harvard Medical School, Boston, Massachusetts 20114

Nociceptive sensory neurons are unusual in expressing voltage-gated inward currents carried by sodium channels resistant to block by tetrodotoxin (TTX) as well as currents carried by conventional TTX-sensitive sodium channels and voltage-dependent calcium channels. To examine how currents carried by each of these helps to shape the action potential in small-diameter dorsal root ganglion cell bodies, we voltage clamped cells by using the action potential recorded from each cell as the command voltage. Using intracellular solutions of physiological ionic composition, we isolated individual components of current flowing during the action potential with the use of channel blockers (TTX for TTX-sensitive sodium currents and a mixture of calcium channel blockers for calcium currents) and ionic substitution (TTX-resistant current measured by the replacement of extracellular sodium by *N*-methyl-D-glucamine in the presence of TTX, with correction for altered driving force). TTX-resistant sodium channels activated quickly enough to carry the largest inward charge during the upstroke of the nociceptor action potential (~58%), with TTX-sensitive sodium channels also contributing significantly (~40%), especially near threshold, and high voltage-activated calcium currents much less (~2%). Action potentials had a prominent shoulder during the falling phase, characteristic of nociceptive neurons. TTX-resistant sodium channels did not inactivate completely during the action potential and carried the majority (58%) of inward current flowing during the shoulder, with high voltage-activated calcium current also contributing significantly (39%). Unlike calcium current, TTX-resistant sodium current is not accompanied by opposing calcium-activated potassium current and may provide an effective mechanism by which the duration of action potentials (and consequently calcium entry) can be regulated.

Key words: action potential; excitability; dorsal root ganglion; nociceptor; sodium channel; tetrodotoxin

Unmyelinated C-fibers originate from small primary sensory neurons and transmit nociceptive information into the CNS. Nociceptive neurons are unusual in expressing voltage-gated sodium current resistant to tetrodotoxin (TTX; Kostyuk et al., 1981) (for review, see McCleskey and Gold, 1999; Waxman et al., 1999), and genes encoding two TTX-resistant (TTX-R) sodium channels, $Na_V1.8$ and $Na_V1.9$, are expressed exclusively in peripheral sensory neurons (Akopian et al., 1996; Dib-Hajj et al., 1998; Amaya et al., 2000). The expression of $Na_V1.8$ has been implicated in mediating inflammatory pain (Akopian et al., 1999; Porreca et al., 1999).

Nociceptive sensory neurons also express TTX-sensitive (TTX-S) sodium channels (Kostyuk et al., 1981; Caffrey et al., 1992; Roy and Narahashi, 1992; Elliott and Elliott, 1993) and multiple types of voltage-dependent calcium channels (Scroggs and Fox, 1992a). It is unknown exactly how each of these three depolarization-activated inward cation currents helps to shape the action potential and contributes to the excitability of the neurons. TTX-R sodium current has much slower activation and inactivation kinetics than the TTX-S sodium current (Kostyuk et al., 1981; Elliott and Elliott, 1993) and is likely to follow a different time course during the action potential. The action potentials of nociceptors associated with C-fibers have unusually wide action potentials with a characteristic hump or shoulder on the falling phase (Gallego, 1983; Ritter and Mendell, 1992; Djouhri et al., 1998; Lopez de Armentia et al., 2000). The shoulder generally has been attributed to calcium current (Dichter and Fischbach, 1977; Ransom and Holz, 1977; Yoshida et al., 1978; Gallego, 1983; Renganathan et al., 2001). Consistent with this, the shoulder is still present in neurons from $Na_V1.8$-null mice (Renganathan et al., 2001). On the other hand, computer modeling has raised the possibility of substantial current from TTX-R channels during the shoulder (Schild and Kunze, 1997). Such modeling depends critically on extrapolated inactivation kinetics at voltages near the peak of the action potential, where kinetics of the current cannot be measured easily, so experimental tests of the predictions of the model would be useful.

Currents flowing during an action potential can be measured directly by using the action potential clamp method (Llinás et al., 1982; McCobb and Beam, 1991; Scroggs and Fox, 1992b) in which an action potential waveform is used as the command voltage in voltage-clamp experiments. This offers a more direct approach than either computer modeling or experiments testing the effect of blockers in current clamp in which the blocking of one current changes the voltage trajectory, producing indirect effects on all other voltage-gated conductances. Ideally, the action potential clamp should be performed with action potentials recorded in the same cell (de Haas and Vogel, 1989; Doerr et al., 1989; Taddese and Bean, 2002) rather than generic action potentials, because there is substantial cell-to-cell variability in current densities and

Received June 29, 2002; revised Sept. 17, 2002; accepted Sept. 24, 2002.

This work was supported by National Institutes of Health Grants HL35034, NS36855, and NS38312. N.T.B. was supported by the Stuart H. Q. and Victoria Quan Fellowship.

Correspondence should be addressed to Nathaniel Blair, Department of Neurobiology, Harvard Medical School, 220 Longwood Avenue, Boston, MA 02115. E-mail: nathaniel_blair@student.hms.harvard.edu.

Copyright © 2002 Society for Neuroscience 0270-6474/02/2210277-14$15.00/0

action potential shapes. Using small dorsal root ganglion (DRG) neurons with electrophysiological properties matching those expected of nociceptors, we used the action potential clamp method with individual neurons to examine the contribution of TTX-sensitive, TTX-resistant, and calcium currents at various times during the action potential.

MATERIALS AND METHODS

Cell preparation. DRG neurons were prepared from Long–Evans rats, postnatal day 14–18. Animals were anesthetized with isoflurane and decapitated, and ganglia were removed and chopped in half. Pieces of ganglia were treated at 37°C for 20 min in 100 U/ml papain (Worthington Biochemical, Lakewood, NJ) with 5 mM cysteine in Ca^{2+}, Mg^{2+}-free Hank's solution containing (in mM): 136.9 NaCl, 5.4 KCl, 0.34 Na_2HPO_4, 0.44 KH_2PO_4, 5.55 glucose, 5 HEPES, and 0.005% phenol red, pH 7.4. After this, the ganglia were transferred to Ca^{2+}, Mg^{2+}-free Hank's solution containing 3 mg/ml collagenase (type I; Sigma-Aldrich, St. Louis, MO) and 4 mg/ml Dispase II (Boehringer Mannheim, Indianapolis, IN) and were incubated for 20 min at 37°C. Ganglia were placed in Leibovitz's L-15 medium (Invitrogen, San Diego, CA) supplemented with 10% fetal calf serum, 5 mM HEPES, and 100 ng/ml NGF (Invitrogen); individual cells were dispersed by trituration with a fire-polished Pasteur pipette and plated on glass coverslips treated with 100 μg/ml poly-D-lysine. Cells were incubated in the supplemented L-15 solution (in room air) at 33°C for 2–4 hr, after which they were stored at 4°C. When used within 48 hr, these cells retained a healthy appearance and had negative resting potentials and overshooting action potentials. There was no obvious systematic difference in action potential parameters between cells used the day of preparation and those kept at 4°C for up to 48 hr.

General electrophysiology. Whole-cell recordings from DRG neurons were made with an Axopatch 200B amplifier (Axon Instruments, Union City, CA). Borosilicate micropipettes (100 μl microcapillaries; VWR, South Plainfield, NJ) or Corning 7052 glass (A&M Systems, Everett, WA) were pulled to resistances of 2.5–5.5 MΩ when filled with the standard potassium methanesulfonate (K-Mes) internal solution containing (in mM): 140 K-Mes, 13.5 NaCl, 1.6 $MgCl_2$, 0.09 EGTA, 9 HEPES, 0.9 glucose, 14 Tris-creatine PO_4, 4 Mg-ATP, and 0.3 Tris-GTP, pH 7.2 (with KOH). In an earlier series of experiments an internal solution lacking Na^+ was used, consisting of (in mM): 135 K-Mes, 1.8 $MgCl_2$, 9 EGTA, 9 HEPES, 14 Tris-creatine PO_4, 4 Mg-ATP, and 0.3 Tris-GTP, pH 7.4 (with KOH). Cells dialyzed with this solution had less negative resting potentials (perhaps because the absence of internal Na^+ eliminates hyperpolarizing current from Na^+–K^+ ATPase activity) as well as more positive action potential peaks (presumably because of an unphysiologically positive sodium equilibrium potential). These cells are not included in the analysis. Seals were formed in Tyrode's solution consisting of (in mM): 150 NaCl, 4 KCl, 2 $CaCl_2$, 2 $MgCl_2$, 10 glucose, and 10 HEPES, pH 7.4 (NaOH); after the whole-cell mode had been established, cells were lifted off the coverslip in front of an array of quartz fiber flow pipes. Pipette tips were wrapped with Parafilm to help in reducing pipette capacitance, which permitted the fast current-clamp mode to be used with lower resistance pipettes than was otherwise possible. In whole-cell voltage-clamp mode the capacity current was removed as much as possible by using the amplifier circuitry, and series resistance compensation was set at 80–95%. Recordings were made within ~25 min after forming whole-cell configuration, because both TTX-R sodium current (Schild and Kunze, 1997) and calcium current showed considerable rundown with longer recordings.

Action potential clamp of DRG neurons. Action potentials were elicited in Tyrode's solution by a short (0.5 msec) current injection. Depolarization to threshold typically was achieved by 1–3 nA for 0.5 msec. Short injections of current were used so that the action potential itself was uncontaminated by injected current. Action potentials were filtered at 10 kHz (−3 dB, four-pole Bessel), digitized at 100 kHz, and used as the command waveform after the amplifier was switched into voltage-clamp mode.

Ionic current separation. The various components of ionic current flowing during the action potential were measured by performing the action potential clamp and by using a pharmacological and ionic substitution strategy to separate the currents. TTX-sensitive sodium current was determined as the current that was sensitive to block by 300 nM TTX, a concentration chosen to block the TTX-sensitive sodium current fully while sparing the TTX-resistant sodium current, which requires ~40 μM for half-block (Roy and Narahashi, 1992; Elliott and Elliott, 1993; Ogata and Tatebayashi, 1993). There was often considerable sweep-to-sweep decline in potassium currents, especially when cells were stimulated at high frequencies. Because of this, action potential commands were applied at low rates (generally 0.1 Hz), and only two to three sweeps in each solution were collected and averaged. Even so, in some cases the TTX-sensitive currents defined by TTX subtraction were sometimes outward, almost certainly because the error resulting from nonstationary potassium currents was larger than any TTX-sensitive sodium current. When the value for TTX-sensitive charge transfer was calculated for the data summarized in Figure 11, a positive (outward) value was considered as zero.

The TTX-R sodium current was isolated by using complete replacement of Na by *N*-methyl-D-glucamine (NMDG), both solutions containing 300 nM TTX to block TTX-S current, as well as a mixture of calcium channel blockers (10 μM nimodipine, 1 μM ω-conotoxin-GVIA, and 250 nM ω-agatoxin (Aga)-IVA) and also 5 mM TEA to reduce potassium currents. Eliminating calcium currents was necessary when measuring TTX-R current by NMDG replacement for Na, because calcium currents themselves are reduced slightly by the substitution of NMDG for Na (Zhou and Jones, 1995); reducing potassium currents was necessary because potassium currents were found to be reduced by 10–15% when NMDG replaced Na.

The high voltage-activated (HVA) calcium current was obtained as the current blocked by a mixture containing 10 μM nimodipine, 1 μM ω-conotoxin-GVIA, and 250 nM ω-Aga-IVA. The calcium channel blocker mixture was applied in external solutions designed to reduce calcium-activated and purely voltage-activated potassium currents, either Tyrode's solution with 5 mM TEA-Cl added or an external solution with Na and K completely replaced with TEA-Cl. In early experiments the HVA calcium current was obtained as the current that was sensitive to block by 30 μM $CdCl_2$. This gave similar results as the calcium channel blocker mixture used in the succeeding experiments, but the blocker mixture was preferred because the block of HVA current by Cd^{2+} is relieved slightly at strongly depolarized and hyperpolarized voltages (Swandulla and Armstrong, 1989) and because Cd^{2+} directly reduces the TTX-resistant sodium current to some extent, as described previously (Ikeda and Schofield, 1987; Roy and Narahashi, 1992). Thus quantification of the contribution of HVA calcium current during the action potential was made with only those cells that were studied using the calcium channel-blocking mixture. The low voltage-activated (LVA) calcium current was defined as the current blocked by the addition of 2 μM mibefradil in the continuous presence of the HVA blocker cocktail.

In some experiments that examined the kinetics and voltage dependence of sodium currents with voltage steps, internal solutions lacking potassium were used to improve the isolation of the currents. One was TEA-based: (in mM), 120 TEA-Cl, 15 NaCl, 1.8 $MgCl_2$, 9 EGTA, 9 HEPES, 14 Tris-creatine PO_4, 4 Mg-ATP, and 0.3 Tris-GTP, pH 7.4; the other was NMDG-based: 130 NMDG, 120 aspartate, 15 NaCl, 1.8 $MgCl_2$, 9 EGTA, 9 HEPES, 14 Tris-creatine PO_4, 4 Mg-ATP, and 0.3 Tris-GTP, pH 7.4 (with 7 mM CsOH). The NMDG-based internal solution also was used in the experiments shown in Figures 7 and 8 examining at high resolution the kinetics and completeness of inactivation of TTX-S and TTX-R currents during an action potential waveform. These experiments used an action potential previously recorded from another cell (chosen to have typical parameters), because it was not possible to record a normal action potential with the NMDG-based internal solution.

Cell selection and classification. Cells were selected for recording on the basis of size and then were tested for the magnitude of several ionic currents that have been proposed to divide DRG neurons into functional groups (Cardenas et al., 1995; Petruska et al., 2000). Images of cells were taken with a CCD camera (Hitachi, Woodbury, NY), captured with a video acquisition card (Scion, Frederick, MD) with a resolution of 0.4 μm, and stored on a computer.

Cells were tested for the magnitude of the hyperpolarization-activated current I_h and the transient potassium current I_A. I_h was measured as the time-dependent current that was activated during a 500 msec step to −130 mV from a holding potential of −60 mV. I_A was measured (during a continuation of the same voltage protocol) as the peak outward current that was activated within the first 60 msec of a step from −130 mV (500 msec) to −60 mV. After the completion of action potential clamp experiments, most cells were tested for sensitivity to capsaicin, prepared fresh daily and applied at 500 nM in Tyrode's solution. The holding current at −70 mV was measured, and cells were designated as capsaicin-

sensitive provided that the inward current increased with application of capsaicin and reversed after the cells were removed from capsaicin. Capsaicin-activated currents ranged from ~5 to 300 pA/pF and showed both sustained and desensitizing patterns.

Solutions and drugs. TTX was from Calbiochem (La Jolla, CA), ω-conotoxin-GVIA was from Bachem (Torrance, CA), ω-Aga-IVA was from Peptides International (Louisville, KY), and mibefradil was a gift from Hoffman-LaRoche (Basel, Switzerland).

Data acquisition and analysis. Currents and voltages were digitized and controlled via a Digidata 1321A interface, controlled by pClamp 8 software (Axon Instruments). Analysis was done with Igor Pro (version π; Wavemetrics, Lake Oswego, OR), with Data Access (Bruxton, Seattle, WA) used to import pClamp files. Cell capacitance was measured by integrating the average of 10–15 current responses to a −10 mV voltage step from −68 mV, filtered at 20 kHz and acquired at 100 kHz. Cell input resistance also was calculated from this average, using the steady-state current change. Reported voltages have been corrected for the −8 mV junction potential between the potassium methanesulfonate-based internal solution and the Tyrode's solution present when zeroing the pipette current. The junction potential was measured by using a flowing 3 M KCl bridge as described by Neher (1992). The NMDG-aspartate internal solution had an offset of −4 mV, which was corrected, whereas the TEA-Cl internal solution had an offset of approximately +1 mV, which was not corrected. Data are presented as the mean ± SD.

RESULTS

Electrophysiological properties of small DRG neurons

Action potentials were recorded from 52 small DRG neurons, which had a mean diameter of 26 ± 3 μm. We used short current injections of 0.5 msec to generate action potentials, leaving most of the action potential free of the effect of injected current (Fig. 1*A*, *top*). Action potentials had positive peaks (+42 ± 4 mV) and long durations when measured at the half-maximal potential (4.7 ± 1.9 msec) (Fig. 2*A,B*). Most action potentials displayed a characteristic inflection, or shoulder, during the repolarization phase. The average resting potential was −76 ± 8 mV, and the average input resistance when measured in voltage clamp was 2.0 ± 1.1 GΩ (Fig. 2*C,D*).

Nearly all cells had properties consistent with identification as nociceptors. The TTX-R sodium current characteristic of nociceptors (Caffrey et al., 1992) was present in 15 of 16 cells that were tested. Cells consistently had large and long-lasting afterhyperpolarizations (AHPs) after action potentials, another feature associated with nociceptive classes of cells (Harper and Lawson, 1985; Djouhri et al., 1998). AHPs that followed action potentials had an amplitude of −84 ± 3 mV (n = 49), and the time required for the AHP to decay by 80% was 307 ± 196 msec (n = 49). (In nine cells the AHP had not decayed by 80% within 550 msec, the longest duration recorded, and a duration of 550 msec was used for statistics.) The long-lasting AHPs probably reflect a combination of slowly decaying potassium conductances together with long membrane time constants.

Cardenas et al. (1995, 1997) and Petruska et al. (2000) have developed a system to classify acutely dissociated DRG neurons into distinct groups on the basis of a combination of properties, including cell diameter, action potential characteristics, and level of expression of ionic currents such as the hyperpolarization-activated cation current I_h, and the transient potassium current

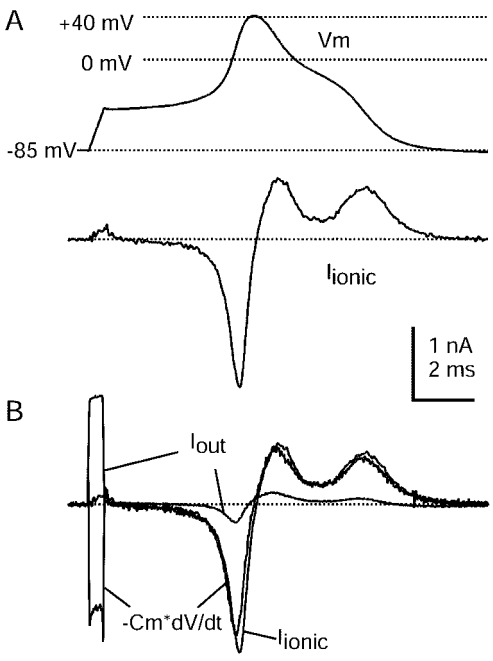

Figure 1. Action potential clamp in small DRG neurons. *A*, *Top*, Action potential elicited in a DRG neuron by a short current injection (1.5 nA for 0.5 msec; timing is the same as I_{out} signal in *B*). *A*, *Bottom*, Ionic current recorded in voltage clamp with the use of the action potential as a command waveform. Capacity current was eliminated by amplifier circuitry. Holding potential was set to the recorded resting potential of the cell of −85 mV. *B*, Comparison of ionic current in voltage clamp (*black*) and the ionic current calculated by scaling the time derivative of the action potential by the measured cell capacitance, 18.7 pF (*gray*). Also shown is the I_{out} signal recorded during the action potential. The action potential was recorded in fast current-clamp mode with bridge balance for electrode series resistance. The *dotted line* shows zero current level. Internal solution contained (in mM): 140 K-Mes, 13.5 NaCl, 1.6 $MgCl_2$, 0.09 EGTA, 9 HEPES, 0.9 glucose, 14 Tris-creatine PO_4, 4 Mg-ATP, and 0.3 Tris-GTP, pH 7.2 (with KOH). External solution was normal Tyrode's solution.

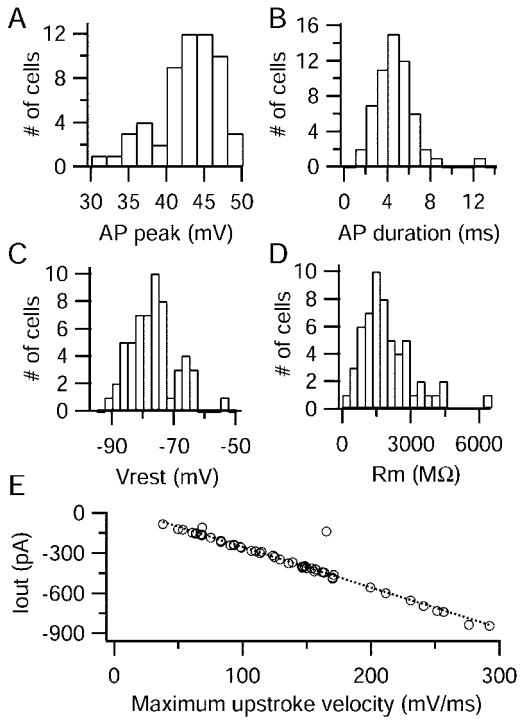

Figure 2. Statistical properties of action potentials in small DRG cells. *A–D*, Amplitude histograms of action potential peak, action potential duration (measured at half-maximal amplitude), resting potential (measured as average of 3–10 sec), and input resistance. *E*, Relationship between the maximal negative I_{out} signal versus the maximal upstroke velocity. The *dotted line* shows the least-squares regression line, with a slope of −3 pA per mV/msec and a *y*-intercept of +48 pA.

I_A. Virtually all of the cells we studied corresponded well with the types of neurons designated types 1 and 2 in their systems in having long-duration action potentials with shoulders and long-lasting AHPs as well as expressing little or no I_h, with an average density of 1.4 ± 1.5 pA/pF (n = 52). Expression of I_A was variable, with 31 of 52 cells expressing <5 pA/pF, corresponding to type 1, and the remaining cells, corresponding to type 2, ranging up to 85 pA/pF (overall 17 ± 25 pA/pF; n = 52). When possible, cells were tested at the end of the experiment for a response to 500 nM capsaicin; from a total of 34 cells that were tested, 25 gave clear responses. There were no systematic differences between capsaicin-sensitive and capsaicin-insensitive cells in action potential shapes, passive membrane properties, or characteristics of sodium and calcium currents, so results were pooled. The correspondence of the characteristics of the cells we studied with type 1 and 2 cells, together with the presence of TTX-R current (in all but one cell), is consistent with their identification as nociceptors corresponding to C-type and Aδ-type fibers (Cardenas et al., 1995, 1997). It is possible that a few cells that we studied with small but detectable I_h would fall into the type 7 classification in the scheme of Petruska et al. (2000), also believed to correspond with a type of nociceptor.

Action potential clamp in small DRG neurons

To measure the ionic currents flowing during action potentials in small DRG neurons, we used the action potential clamp technique. We first recorded the action potential of each cell in current clamp, switched to voltage-clamp mode, and used that waveform as the command voltage. During a free-running action potential in an isopotential cell, the ionic current, I_{ionic}, acts to charge the cell capacitance so that the total current, $I_{ionic} + C_m dV/dt$, is equal to zero (Hodgkin and Huxley, 1952). Thus net ionic current flowing during the action potential can be calculated from $-C_m dV/dt$. During an action potential clamp the timing of membrane voltage, capacity current, and ionic current should be the same as during a free-running action potential. Thus, if there were ideal recording in both current-clamp and voltage-clamp modes and perfect stationarity of membrane properties, the ionic current elicited by the action potential clamp should be equal to $-C_m dV/dt$. This was tested in the experiment shown in Figure 1. Ionic current elicited by the action potential clamp was recorded by using the capacitance compensation circuitry of the amplifier to remove capacity current (Fig. 1*A*). The elicited ionic current was quite similar to that calculated from $-C_m dV/dt$ of the action potential waveform (Fig. 1*B*). On average, peak membrane ionic current recorded under voltage clamp was 16 ± 13% (n = 48) larger than that calculated from the time course of the action potential and cell capacitance.

Action potentials recorded with patch-clamp amplifiers can be distorted significantly, because the current-clamp mode of such amplifiers requires a feedback circuit for which the bandwidth is limited (Magistretti et al., 1996, 1998). The extent of the distortion can be estimated from the deviation from zero in the actual current flowing in the headstage, which can be large (several nanoamps) when feedback bandwidth is limited. We made all recordings by using the fast current-clamp mode of the Axopatch 200B amplifier, with increased bandwidth, and previous measurements suggest that distortion of the action potential is minimal in this mode (Magistretti et al., 1998). Consistent with this, the maximal measured headstage current (I_{out}) during the current-clamp recording was always <1 nA, averaging −345 ± 212 pA (n = 48). Peak inward I_{out} ranged from 90 to 840 pA and was proportional to the maximal upstroke of the action potential, closely approximated by the relation:

$$I_{out} = -3dV/dt,$$

where I_{out} is in pA and dV/dt is in millivolts per millisecond (Fig. 2*E*). I_{out} was always small in relation to total peak ionic current measured during the upstroke of the action potential, averaging 10 ± 4%. This comparison suggests that distortions of the recorded action potentials are minimal and that they can be used appropriately as voltage commands.

The fact that peak ionic current recorded under voltage clamp was somewhat larger than that calculated from the action potential can be rationalized in terms of the modest distortion of the action potential. Because of the imperfection in current clamp, the upstroke of the action potential is somewhat less steep than it would be if measured perfectly (Magistretti et al., 1996), thus reducing the peak ionic current calculated from $-C_m dV/dt$. In addition, when this action potential is used as the command in voltage clamp, the slower rate of rise would allow more complete activation of the sodium current. Thus the imperfect current clamp would result in an underestimate of $-C_m dV/dt$ and an overestimate of peak sodium current, consistent with the results. The average difference of 16% seems consistent with a distortion of the action potential rate of rise by ~10%. The analysis suggests that it is possible to quantify sodium currents even during the upstroke of the action potential with reasonable accuracy.

Multiple sodium currents in small DRG neurons

The ionic current flowing during the upstroke of the action potential presumably is primarily sodium current. Nociceptors are unusual in expressing multiple TTX-R sodium channels in addition to the more conventional TTX-S sodium channels (for review, see McCleskey and Gold, 1999; Waxman et al., 1999). Figure 3 illustrates the effect of TTX on total voltage-gated sodium current elicited by step depolarizations, recorded with ionic conditions designed to isolate sodium current (internal TEA^+ to block potassium currents and external 30 μM Cd^{2+} to block calcium currents). TTX at 300 nM blocked some, but not all, of the sodium current. As expected, the currents carried by TTX-R sodium channels had distinct functional properties, with approximately fivefold slower activation and inactivation kinetics compared with the TTX-S sodium current. In addition to different kinetics the TTX-R sodium current has considerably different voltage dependence than the TTX-S sodium current, as observed previously (Kostyuk et al., 1981; Roy and Narahashi, 1992; Elliott and Elliott, 1993). The TTX-R current in the cell shown in Figure 3 required slightly more depolarized voltages to open, with the midpoint of activation shifted ~5 mV. There was a much larger difference in the voltage dependence of inactivation, with the midpoint for TTX-R current shifted in this cell by ~40 mV in the depolarizing direction. Thus at voltages between −75 and −50 mV there is considerable steady-state inactivation of TTX-S sodium current but very little of TTX-R sodium current. In collected results that used the TEA-Cl internal solution and Tyrode's solution with 30 μM Cd^{2+} as the external solution, the midpoint of activation of TTX-R current was −15 ± 4 mV (n = 8), and the midpoint of inactivation was −35 ± 4 mV (n = 13).

Rush and colleagues (1998) distinguished in different DRG neurons two TTX-resistant sodium currents with different voltage dependence and kinetics. In our experiments the properties of the TTX-R current were consistent from cell to cell, and we had no clear indication of two distinct types. Comparison of the voltage

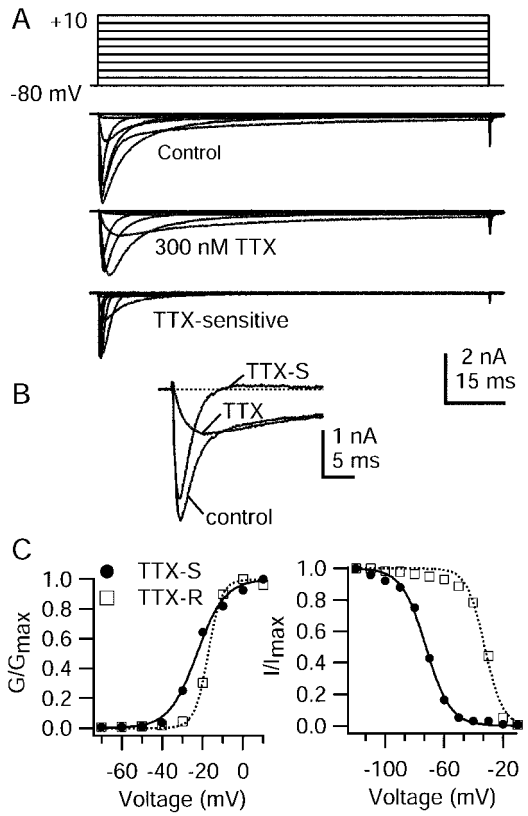

Figure 3. TTX-sensitive and TTX-resistant voltage-gated sodium currents in DRG neurons. *A*, Currents elicited by 100 msec steps from a holding potential of −80 mV to voltages between −70 and +10 mV in 10 mV increments. Internal solution contained (in mM): 120 TEA-Cl, 15 NaCl, 1.8 $MgCl_2$, 9 EGTA, 9 HEPES, 14 Tris-creatine PO_4, 4 Mg-ATP, and 0.3 Tris-GTP, pH 7.4. External solution was Tyrode's solution with 30 μM $CdCl_2$ and 5 mM TEA-Cl. *A*, *Top*, Control. *A*, *Middle*, After the addition of 300 nM TTX. *A*, *Bottom*, TTX-sensitive current obtained by subtraction. *B*, Currents (same as in *A*) elicited during −20 mV step in control, 300 nM TTX, and resulting subtraction (*TTX-S*) shown on an expanded time base. The *dotted line* shows zero current level. *C*, *Left,* Voltage dependence of peak conductance for TTX-S (*filled circles*) and TTX-R (*open squares*) sodium currents (same cell as in *A*). Conductance (G) was calculated as $G = I/(V - V_{rev})$, in which I is the peak current, V is the voltage, and V_{rev} is the reversal potential for sodium channel current (taken as +58 mV). G is plotted normalized to G_{max}, the peak conductance for a step to +10 mV. *Filled circles*, TTX-S current; *open squares*, TTX-R current. The *lines* are best fits to the Boltzmann function:

$$1/(1 + \exp[-(V - V_{½})/k]),$$

where V is the step membrane potential in millivolts, $V_{1/2}$ is the half-maximal voltage in millivolts, and k is the slope factor in millivolts. TTX-S (*solid line*), $V_{1/2} = -22.8$ mV and $k = 6.9$ mV; TTX-R (*dotted line*), $V_{1/2} = -17.3$ mV and $k = 3.4$ mV. *C*, *Right*, Voltage dependence of inactivation determined by using 500 msec prepulses and test pulses to −10 mV. Test pulse current is normalized to its maximal value. *Solid curves* are best fits to the Boltzmann function:

$$1/(1 + \exp[(V - V_{½})/k]),$$

where V is the prepulse membrane potential, $V_{1/2}$ is the half-maximal voltage, and k is the slope factor in millivolts. TTX-S (*solid line*), $V_{1/2} = -72.3$ mV and $k = 8.2$ mV; TTX-R (*dotted line*), $V_{1/2} = -32.4$ mV and $k = 6.1$ mV.

dependence and kinetics of our TTX-R current with those of Rush et al. (1998) is difficult because both internal and external solutions were different in significant ways. Our solutions were more similar (but not identical) to those of d'Alcantara et al. (2002), who characterized TTX-resistant current in a specific population of rat DRG neurons (type 2 in the Cardenas-Petruska system) and concluded that it corresponded to the TTX-R2 current of Rush et al. (1998), which has a more negative voltage dependence of activation than the TTX-R1 current. The midpoint of activation of the TTX-R current in our experiments (−15 mV) was somewhat more negative than that (0 mV) of d'Alcantara et al. (2002), suggesting that it corresponds better to TTX-R2 than to TTX-R1 current. Consistent with this, the TTX-R sodium current in our experiments showed pronounced use dependence, declining 25–55% after 10 pulses applied at 1 Hz from a holding potential of −60 mV, similar to both the TTX-R2 subtype of Rush et al. (1998) and the current recorded in type 2 DRG neurons by d'Alcantara et al. (2002).

TTX-sensitive sodium current during the action potential

The different kinetics and voltage dependence of the TTX-S and TTX-R sodium currents suggest that their contributions to the action potential will be different. Using the action potential clamp, we directly recorded the TTX-S and TTX-R currents flowing during the action potential of each cell. Figure 4*A* shows the result observed in the majority of DRG cells from which we recorded, in which the TTX-S sodium currents overall were quite small. The TTX-S sodium current activated during the initial depolarization in the voltage command waveform and then rapidly declined before the action potential reached its peak value. This decline in current was partly a result of the decreased driving force as the voltage approached the sodium equilibrium potential. In addition, the sodium channels were likely to be inactivating. As the action potential repolarized, TTX-S sodium current remained near zero, while the driving force for sodium increased, suggesting that inactivation of TTX-S sodium channels was nearly complete by the time of the falling phase.

In most cells from which we recorded, the current during the upstroke blocked by TTX was smaller than that remaining in TTX, but there were a few cells in which TTX-S current was dominant. Records from one such cell are shown in Figure 4*B*. The larger magnitude of the TTX-S sodium current in this cell allowed for a more accurate TTX subtraction and higher resolution of its time course during the action potential. In agreement with Figure 4*A*, the larger TTX-S current in Figure 4*B* reached its maximum during the early rising phase of the action potential and was inactivated completely during the falling phase of the action potential. Overall, of the 13 cells in which all of the major inward currents were quantified simultaneously, there were five in which the majority of inward current during initial upstroke was contributed by the TTX-S sodium current. This current was always near zero during the falling phase of the action potential.

One of these five cells expressed TTX-S current exclusively, because the addition of 300 nM TTX completely abolished the inward current during the action potential. This cell had an unusually narrow action potential (1.0 msec at half-maximal amplitude), was not sensitive to 500 nM capsaicin, did not express I_A, and expressed a large I_h current. These observations all suggest that the anomalous cell was likely a type 3 or 4 cell (Cardenas et al., 1995).

TTX-resistant sodium current during the action potential

To isolate accurately the TTX-R sodium current during the action potential of a cell, we found that it was necessary to find a

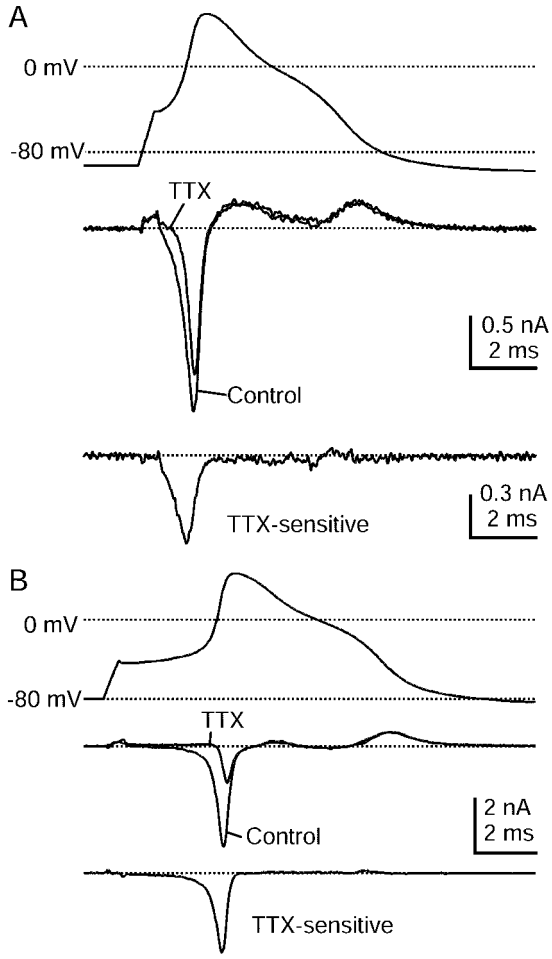

Figure 4. Time course of TTX-S sodium current during the action potential as measured with physiological solutions. *A*, *Top*, Action potential recorded from a DRG neuron 23 μm in diameter. *A*, *Middle*, Currents (single sweeps) recorded during action potential clamp in control Tyrode's solution (*black*) and after the addition of 300 nM TTX (*gray*). The *dotted line* indicates zero current level. *A*, *Bottom*, TTX-S current derived by subtraction of traces before and after TTX, shown at an increased resolution. *B*, Currents recorded in a cell 29 μm in diameter that had a larger TTX-S sodium current. Currents are averages of three sweeps. Internal solution contained (in mM): 140 K-Mes, 13.5 NaCl, 1.6 $MgCl_2$, 0.09 EGTA, 9 HEPES, 0.9 glucose, 14 Tris-creatine PO_4, 4 Mg-ATP, and 0.3 Tris-GTP, pH 7.2 (with KOH). External solution was Tyrode's solution with or without 300 nM TTX.

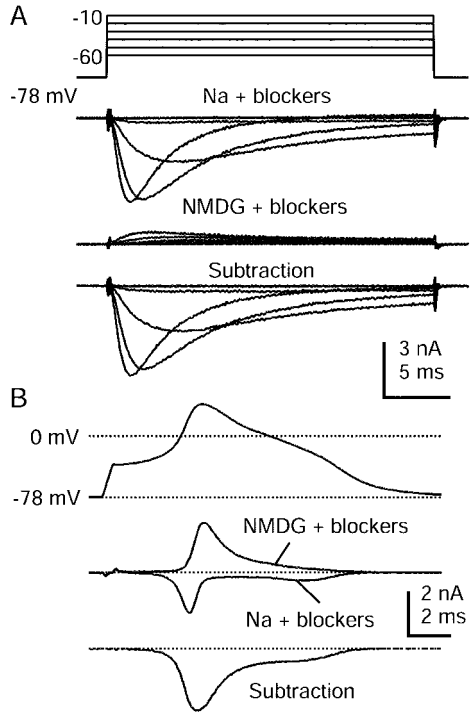

Figure 5. TTX-R sodium current isolated by using NMDG substitution. *A*, Currents in response to voltage steps between −60 and −10 mV, recorded in Tyrode's solution with 300 nM TTX, 5 mM TEAC-l, 10 μM nimodipine, 1 μM ω-conotoxin-GVIA, and 250 nM ω-agatoxin-IVA (*top*). Shown are currents recorded after Na^+ was replaced completely by $NMDG^+$ (*middle*) and the resulting subtraction showing isolated TTX-R sodium current (*bottom*). *B*, Same current isolation procedure used during the action potential clamp in a 27 μm cell. Shown are action potential waveform (*top*), currents in Na and NMDG with blockers (*middle*), and a subtraction yielding raw TTX-R sodium current (*bottom*). Currents are averages of three sweeps. *Na + blockers* solution was Tyrode's solution with 300 nM TTX, 5 mM TEA-Cl, 10 μM nimodipine, 1 μm ω-conotoxin-GVIA, and 250 nM ω-Aga-IVA. *NMDG + blockers* was identical but with NMDG-Cl completely replacing NaCl. Internal solution contained (in mM): 140 K-Mes, 13.5 NaCl, 1.6 $MgCl_2$, 0.09 EGTA, 9 HEPES, 0.9 glucose, 14 Tris-creatine PO_4, 4 Mg-ATP, and 0.3 Tris-GTP, pH 7.2 (with KOH).

subtraction procedure that could be used with a physiological K^+-based internal solution, required for the initial recording of the action potential. We used an ionic substitution approach, replacing all external Na with the impermeant cation NMDG (Fig. 5). The external solution contained 300 nM TTX to block TTX-S sodium current and a calcium channel blocker mixture (10 μM nimodipine, 1 μM ω-conotoxin-GVIA, and 250 nM ω-Aga-IVA) to block voltage-dependent calcium currents. In initial experiments we found that voltage-activated potassium currents were reduced by 10–15% when Na was replaced by NMDG. We therefore added 5 mM TEA-Cl to both the Na and NMDG external solutions. This greatly reduced the potassium currents and minimized the differences between Na- and NMDG-based solutions. Figure 5*A* shows the NMDG subtraction procedure for currents during step depolarizations. The currents obtained by NMDG subtraction have similar voltage dependence and kinetics as the TTX-R sodium currents recorded with a TEA-Cl-based internal solution to block potassium currents (Fig. 3*A*). The midpoint of the activation curve from NMDG-subtracted currents was −18 ± 6 mV ($n = 8$), similar to that from experiments in which TTX-R sodium current was isolated by using TEA-Cl internal solutions (−15 ± 4 mV; $n = 8$). Also, the kinetics of TTX-R currents obtained by the two methods were quite similar. Thus the NMDG subtraction procedure appeared to yield good isolation of TTX-R sodium current even with K^+-based internal solutions.

Figure 5*B* shows currents recorded during action potential clamp, from the same cell as Figure 5*A*, in Na Tyrode's solution with 300 nM TTX, 5 mM TEA-Cl, and the mixture of HVA calcium current blockers added (*top*), after the substitution of Na by NMDG (*middle*), and the resulting subtraction (*bottom*). Appreciable TTX-R current flowed during the earliest phases of the action potential waveform and reached a maximal amplitude during the upstroke. Substantial TTX-R current continued to flow during the inflection on the falling phase, showing that its depolarizing influence contributed to generating the shoulder. All cells that expressed significant TTX-R sodium current dis-

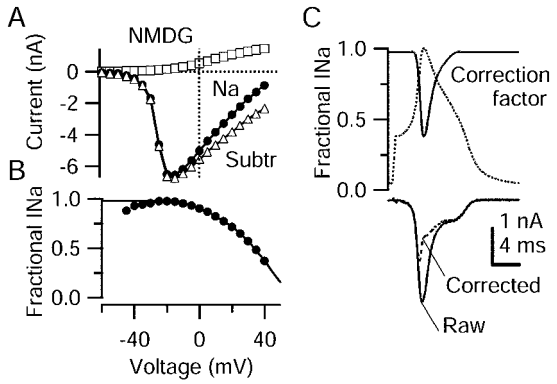

Figure 6. Correction process for NMDG subtraction method. *A*, Peak sodium current as a function of voltage, recorded in Na Tyrode's solution (*filled circles*) or in NMDG Tyrode's solution (*open squares*), each with 30 μM $CdCl_2$ and 5 mM TEA added. Internal solution was designed to block potassium currents completely (in mM): 120 TEA-Cl, 15 NaCl, 1.8 $MgCl_2$, 9 EGTA, 9 HEPES, 14 Tris-creatine PO_4, 4 Mg-ATP, and 0.3 Tris-GTP, pH 7.4. *Open triangles* show the subtraction current. *B*, Ratio of current in Na Tyrode's solution (true sodium current) to the current obtained by NMDG subtraction (too big because of outward sodium current after NMDG substitution). The correction factor (*solid line*) was generated by curve fitting and extrapolating, extending the calculated value at −25 mV (0.98) to −80 mV and extending a straight line from +35 to +50 mV. *C*, *Top*, Correction factor during action potential. *C*, *Bottom*, Raw (*solid line*) and corrected (*dashed line*) TTX-R sodium currents obtained from NMDG subtraction. Traces in *C* are from the same cell as in Figure 5.

played this pattern. The shoulder of the action potential in DRG neurons generally has been ascribed to calcium current, but it is clear from these experiments that the TTX-R sodium current also contributes a large amount of depolarizing current during the falling phase of the action potential, apparently because its inactivation remains incomplete.

Replacing Na by NMDG shifts the sodium current reversal potential in the hyperpolarizing direction, and with 13.5 mM Na^+ in the internal solution a small outward Na current is expected to flow when TTX-R sodium channels are activated. This outward current is evident in the middle panel of Figure 9*A* for step depolarizations to −20 and −10 mV. Such current will be larger for the even larger depolarizations reached during the action potential (up to +40 mV). Thus, subtracting the current recorded in NMDG Tyrode's solution from the current in Na Tyrode's solution will result in an overestimate of net inward current through TTX-R sodium channels, with larger errors at more depolarized voltages. We therefore devised a method to correct for this error. Figure 6 shows the experimental procedure we used to calculate a voltage-dependent correction factor. Figure 6*A* shows current–voltage curves of peak TTX-R current elicited by step depolarizations from −60 to +40 mV either in normal Na Tyrode's solution (Fig. 6*A*, *filled circles*) or after the replacement of Na by NMDG (Fig. 6*A*, *open squares*). TTX-R sodium current was recorded in isolation by using a TEA-Cl-based internal solution with 300 nM TTX, 30 μM $CdCl_2$ and 5 mM TEA-Cl in the external solution. When Na was replaced by NMDG, the TTX-R current was small and outward at all voltages, as expected. Subtracting currents in NMDG Tyrode's solution from those in Na Tyrode's solution yields the raw NMDG subtraction currents (Fig. 6*A*, *open triangles*). This procedure corresponds to the measurement made by using NMDG subtraction with K^+-based internal solutions (Fig. 5). We then calculated a correction factor relating the current measured by this subtraction to inward sodium current in normal Na Tyrode's solution by taking the ratio of the current in Na to the current obtained by NMDG subtraction (Fig. 6*B*). This correction factor (Fig. 6*B*) is a function of voltage. At potentials from −30 to 0 mV the correction factor is close to 1, and it decreases as the potential approaches the sodium equilibrium potential in Na Tyrode's solution. Here the subtraction current is dominated by the outward flow of Na^+ in NMDG Tyrode's solution. To extend the correction factor beyond +40 mV, we extrapolated a straight line from the measured values at +35 and +40 mV. From this line the correction value at +50 mV was 0.15, and it reached zero at +60 mV, very close to the calculated value of the Na equilibrium potential of +58 mV. At this point the current in Na Tyrode's solution no longer contributes, and all current resulting from the subtraction must be attributable to outward current in NMDG Tyrode's solution.

Then the NMDG subtraction current elicited during action potential clamp was multiplied by the voltage-dependent correction factor to yield the corrected TTX-R sodium current (Fig. 6*C*). As expected from the voltage dependence of the correction factor, the raw and corrected currents were essentially identical during the initial upstroke and during much of the shoulder of the repolarizing phase. Larger differences were present during the most positive points in the action potential, where the peak of the corrected TTX-R sodium current occurs earlier than that of the raw current, very near to when the action potential achieves maximal *dV/dt*.

Time course of TTX-S and TTX-R sodium current during the action potential

When studied with physiological internal solutions and the action potential of the cell as the command, the TTX-S and TTX-R sodium currents always had dramatically different time courses during the action potential, with TTX-S current flowing earlier but also terminating earlier. To compare time courses of the TTX-S and TTX-R sodium currents flowing during an action potential with the best temporal resolution and to evaluate the time course of inactivation of the two currents during an action potential, we did a series of experiments in which solutions were changed to enhance the isolation of the sodium current (Fig. 7). A pipette solution with NMDG as the main cation was used to eliminate potassium currents. In these experiments an action potential prerecorded from a different cell was used as the command waveform; for this, we chose an action potential with typical parameters, including a prominent shoulder. Figure 7*A* compares the time course of the TTX-R current with that of the TTX-S sodium current, calculated as the subtraction of currents before and after the addition of 300 nM TTX. As in Figure 3, recorded with more physiological solutions but with less precise resolution, the TTX-S sodium current rapidly activated during the rising phase of the action potential and then declined as the peak of the action potential approached. By this point the TTX-S current was inactivated completely, because the sodium current did not increase as the action potential repolarized. In contrast, the TTX-R sodium current was active throughout the entire action potential duration. With these experimental solutions the TTX-R sodium current can be recorded directly, without the need for a correction factor. The time course of the directly measured TTX-R current during the action potential was very similar to the TTX-R sodium current calculated by NMDG subtraction and the correction procedure (Figs. 5, 6); the current increased during the initial phase of the action potential and decreased as the peak (and thus the sodium equilibrium potential) was approached. As the action

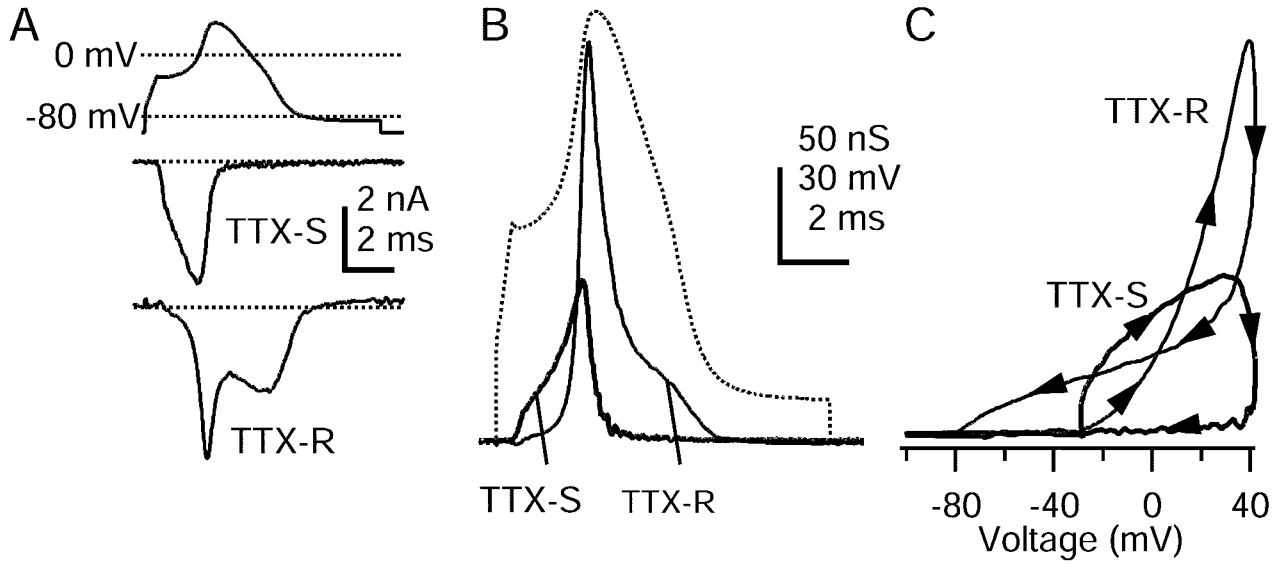

Figure 7. High resolution recording of TTX-S and TTX-R sodium currents flowing during the action potential with the use of internal solution to block potassium currents. Experiments used a previously recorded action potential from a different cell. *A*, TTX-S and TTX-R currents elicited by the action potential waveform. TTX-S current was calculated as a current blocked by 300 nM TTX, averaged over three sweeps. Internal solution contained (in mM): 130 NMDG, 120 aspartate, 15 NaCl, 1.8 $MgCl_2$, 9 EGTA, 9 HEPES, 14 Tris-creatine PO_4, 4 Mg-ATP, and 0.3 Tris-GTP, pH 7.4 (with 7 mM CsOH). External solution was (in mM): 150 NaCl, 4 CsCl, 2 $BaCl_2$, 0.3 $CdCl_2$, 10 glucose, and 10 HEPES, pH 7.4. TTX-R sodium current was recorded in a different cell; leak and capacity current was removed by subtraction of the appropriately scaled current elicited by a scaled (0.2), inverted action potential. Shown is an average of two sweeps, digitally filtered at 5 kHz. The *dotted lines* indicate zero current level. External solution contained (in mM): 150 NaCl, 4 CsCl, 2 $CaCl_2$, 2 $MgCl_2$, 0.03 $CdCl_2$, 5 TEA-Cl, 10 glucose, and 10 HEPES, pH 7.4, with 300 nM TTX. *B*, Time course of TTX-S and TTX-R sodium conductances during the action potential, calculated by dividing the currents recorded in *A* by the driving force on sodium, assuming a sodium equilibrium potential of +60 mV. *C*, TTX-S and TTX-R sodium conductances from *B* plotted against voltage during the action potential. Vertical scale is the same as in *B*.

potential repolarized, the current increased again, indicating that TTX-R sodium channels were not inactivated completely during the initial falling phase of the action potential.

The increase in TTX-R sodium current during the shoulder of the repolarization could be simply a result of the increased driving force on sodium as the action potential repolarizes. Alternatively, it also could be that activation of the channels is slow enough that the sodium conductance continues to increase after the peak of the action potential is reached. To evaluate these factors, we calculated the TTX-S and TTX-R sodium conductances during the action potential by dividing each current by the driving force on sodium (assuming a sodium equilibrium potential of +60 mV) (Fig. 7*B*). As expected, the TTX-S sodium conductance activated quickly and had returned to zero by the peak of the action potential. In contrast, the TTX-R sodium conductance continued to increase after the TTX-S sodium conductance had begun to decrease. In addition, the TTX-R sodium conductance remained active long into the repolarization of the action potential, when the membrane voltage returned near the resting value. This difference in time course of the two types of current is especially apparent when the TTX-S and TTX-R sodium conductances are plotted against membrane potential (Fig. 7*C*). The TTX-S sodium conductance activated quickly, began to decrease near the peak of the action potential, and remained inactive throughout the entire repolarization of the action potential. The TTX-R sodium conductance activated more slowly and also decreased near the peak of the action potential, but the TTX-R sodium conductance remained active even at potentials from −30 to −70 mV during the falling phase of the action potential. Evidently, deactivation of the TTX-R sodium current is slow enough in the later phases of the action potential that it does not turn off completely until the action potential has repolarized to −80 mV.

The different time courses of TTX-S and TTX-R sodium currents suggest that they have different patterns of inactivation during the action potential. To monitor directly the degree of inactivation reached by the TTX-S and TTX-R sodium channels during the action potential, we used a voltage protocol in which progressively more complete fractions of the action potential in Figure 7 were used as a "prepulse" before a 2.5 msec test step to 0 mV (Fig. 8). The sodium current flowing during the test step reflects channels that just before the test step were closed but available to open, together with any channels that were already open just before the test pulse. Twelve different waveforms were used, with the action potential interrupted by a test step at twelve different points throughout its duration. For clarity, the currents elicited by only three of these are illustrated in Figure 8*A*. Interrupting the action potential near the peak elicited large TTX-S and TTX-R sodium tail currents, which then inactivated (Fig. 8*A*, *blue traces*). After the action potential had, in large part, repolarized, the 0 mV test step elicited no additional TTX-S sodium current; evidently, TTX-S sodium channels had inactivated, and there was insufficient time for recovery from inactivation (Fig. 8*A*, *red trace*). Inactivation of the TTX-R sodium current was not as complete at this point in the action potential, because the test step did elicit substantial TTX-R sodium current. Including a short segment of the afterhyperpolarization resulted in some recovery of TTX-S sodium current, to ~20% of its initial value, whereas the TTX-R sodium current recovered from inactivation much more quickly, to ~90% of its initial value (Fig. 8*A*, *black traces*).

The degree of inactivation of each current at each point during

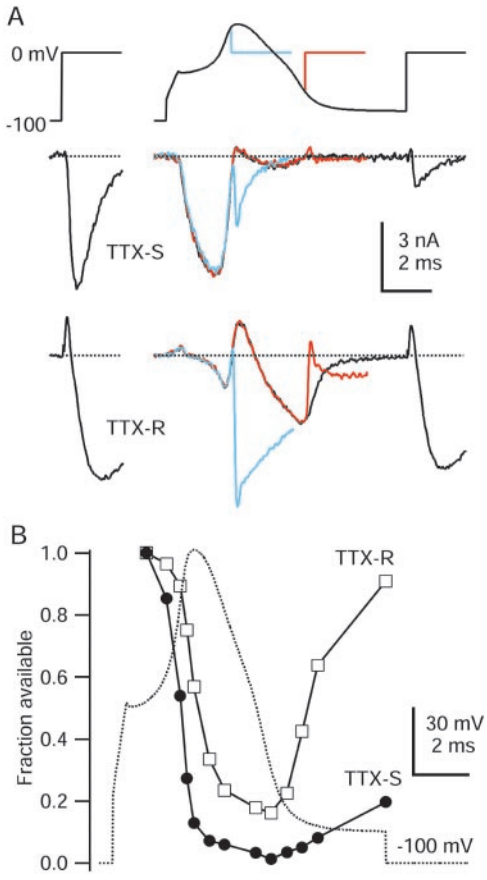

Figure 8. Time course of inactivation of TTX-S and TTX-R sodium currents during the action potential. *A*, *Top*, Three command waveforms consisting of varying durations of a typical action potential (same as Fig. 7) preceding a test step to 0 mV. *A*, *Middle*, TTX-S sodium current. *A*, *Bottom*, TTX-R sodium current (note that outward currents during the peak of the action potential are outward sodium currents resulting from reduced external sodium concentration). For comparison, TTX-S and TTX-R sodium currents elicited during a step from −100 to 0 mV are shown at *left*. External solution for TTX-S current recording was (in mM): 50 NaCl, 100 TEA-Cl, 2 $BaCl_2$, 0.3 $CdCl_2$, 10 glucose, and 10 HEPES, pH 7.4, and for TTX-R current recording was (in mM): 50 NaCl, 100 TEA-Cl, 4 CsCl, 2 $CaCl_2$, 2 $MgCl_2$, 0.03 $CdCl_2$, 10 glucose, and 10 HEPES, pH 7.4, with 300 nM TTX. Internal solution for both contained (in mM): 130 NMDG, 120 aspartate, 15 NaCl, 1.8 $MgCl_2$, 9 EGTA, 9 HEPES, 14 Tris-creatine PO_4, 4 Mg-ATP, and 0.3 Tris-GTP, pH 7.4 (with 7 mM CsOH). *B*, Time course of TTX-S and TTX-R sodium current availability changes during an action potential. Sodium current was measured during the 0 mV test step, reflecting both channels closed but available to being open and also channels already open at the beginning of the test pulse (the two together constituting "available" channels). Test pulse current was normalized to the first test step current and was plotted against the time of test step onset. TTX-S current amplitude was measured 0.62 msec after the initiation of the 0 mV test step; TTX-R current was measured 1.75 msec after test step initiation.

the action potential was monitored as the relative size of the test pulse current (Fig. 8*B*). The TTX-S sodium current was inactivated rapidly early in the action potential, with inactivation substantially complete by the time of the peak of the action potential (81 ± 5%; $n = 6$) and complete inactivation reached near the end of the action potential repolarization (98 ± 2%; $n = 6$). Recovery from inactivation of the TTX-S sodium current began when the action potential had repolarized to near −70 mV. However, the TTX-S sodium current was slow to recover, with 76 ± 17% ($n = 6$) of the current remaining inactivated ~4 msec later.

The TTX-R sodium current inactivated more slowly and less completely than the TTX-S sodium current did. At the peak of the action potential, TTX-R sodium current inactivation was only 41 ± 13% ($n = 5$) complete, and maximal inactivation at the end of the action potential was 78 ± 13% ($n = 5$) complete. The recovery of the TTX-R sodium current was much more rapid than that of the TTX-S current, recovering nearly completely just ~4 msec after the time of maximal inactivation (10 ± 2% inactivated; $n = 5$). This dramatic difference in TTX-S and TTX-R sodium current recovery from fast inactivation during the action potential fits well with previous studies examining recovery at fixed potentials (Elliott and Elliott, 1993; Schild and Kunze, 1997; but see Ogata and Tatebayashi, 1993).

Calcium currents during the action potential in small DRG neurons

To examine the contribution of high voltage-activated calcium current during the action potential, we made recordings that used the K^+-based internal solution and isolated calcium currents defined by subtraction, as the current that was sensitive to the addition of a mixture of 10 μM nimodipine, 1 μM ω-conotoxin-GVIA, and 250 nM ω-Aga-IVA. Subtractions were done with an external solution of 160 mM TEA-Cl and 300 nM TTX (to minimize calcium-activated potassium currents, voltage-dependent potassium currents, and sodium currents) or in Tyrode's solution with 300 nM TTX and 5 mM TEA-Cl added. Figure 9*A* shows currents elicited by step depolarizations before and after additions of calcium current blockers in 160 mM TEA-Cl external solution. There was an initial transient outward current, most likely Na^+ exiting through TTX-R sodium channels, followed by a sustained inward current that did not inactivate over ~100 msec. Application of the calcium current blockers (Fig. 9*A*) had no effect on the transient outward current but abolished the sustained inward current. Judging by the completeness of block of the current at the end of the pulse, the mixture of blockers was sufficient to block essentially all of the calcium current. This is consistent with previous observations that a large fraction of the HVA calcium current in small DRG cells is L- and N-type current (Scroggs and Fox, 1992b; Cardenas et al., 1995), and the results suggest that the remaining HVA current in small-diameter DRG neurons is carried mainly by P/Q-type channels (Mintz et al., 1992). The subtracted current (Fig. 9*A*, *bottom*) showed very little decay over 100 msec and had fast tail currents. Figure 9*B* shows the results of the calcium current isolation procedure during the action potential clamp in the same cell as Figure 9*A*. The initial outward current flowing during the rising phase of the action potential (both in control and with blockers) is very likely outward Na^+ current through TTX-R channels, as in the step depolarizations. The HVA calcium current defined by the blocking mixture began to flow to a small extent during the upstroke of the action potential, decreasing as the action potential neared its peak. This small early calcium current during the rising phase was present in some cells, but not other others (Fig. 10). In all cells a much larger calcium current flowed as the action potential repolarized and as the calcium driving force increased. The time course of the calcium current flow during these recorded action potentials is similar to previous results that used idealized action potential waveforms (McCobb and Beam, 1991; Scroggs and Fox, 1992b; Park and Dunlap, 1998).

In some cells a small amount of net inward current continued to flow during the repolarizing phase of the action potential in the presence of TTX, the NMDG replacement of Na, and the HVA

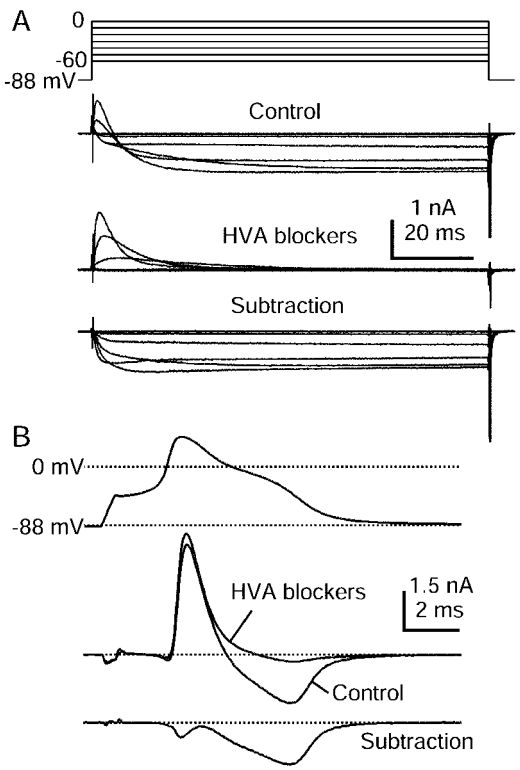

Figure 9. HVA calcium currents elicited by action potential clamp in small DRG cells. *A*, Currents elicited by step depolarizations in control (*top*) and then after the application of 10 μM nimodipine, 1 μM ω-conotoxin-GVIA, and 250 nM ω-Aga-IVA (*middle*). Internal solution contained (in mM): 140 K-Mes, 13.5 NaCl, 1.6 $MgCl_2$, 0.09 EGTA, 9 HEPES, 0.9 glucose, 14 Tris-creatine PO_4, 4 Mg-ATP, and 0.3 Tris-GTP, pH 7.2 (with KOH). External solution for initial recording of action potential was Tyrode's solution. External solution for recording calcium current contained (in mM): 160 TEA-Cl, 2 $CaCl_2$, 2 $MgCl_2$, and 10 HEPES, pH 7.4. Note outward Na current exiting through TTX-R sodium channels. Subtraction of currents with and without blockers yields the HVA calcium current (*bottom*). In these traces 120 μsec after the voltage step has been blanked to remove uncompensated capacitive current. *B*, Subtraction procedure during action potential clamp (same cell as in *A*). Currents recorded in 160 TEA-Cl external solution (*black*) and in the presence of HVA blocker mixture (*gray*) are shown in the *middle*. The resulting subtraction (*bottom*) shows that most HVA calcium current flows during the shoulder in the action potential. Currents are the average of three sweeps.

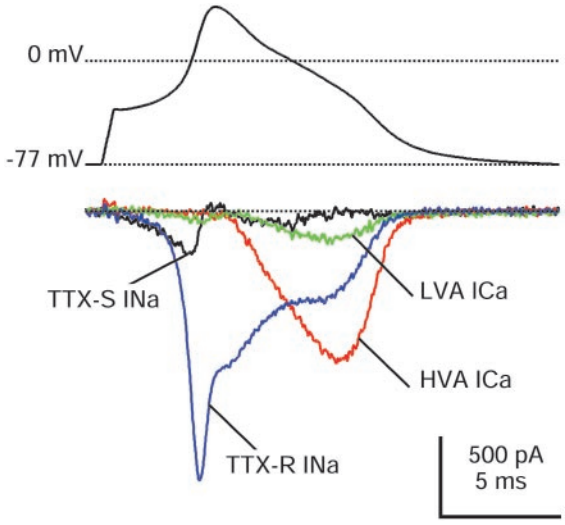

Figure 10. Comparison of different inward currents during action potential clamp recorded in a single DRG neuron (same as Fig. 5). The action potential was recorded and used as command potential, and TTX-S sodium (*black*), TTX-R sodium (*blue*), HVA calcium (*red*), and LVA calcium (*green*) currents were isolated as detailed in Results. This cell had a resting potential of −86 mV when averaged over a longer duration before the action potential was recorded. Internal solution contained (in mM): 140 K-Mes, 13.5 NaCl, 1.6 $MgCl_2$, 0.09 EGTA, 9 HEPES, 0.9 glucose, 14 Tris-creatine PO_4, 4 Mg-ATP, and 0.3 Tris-GTP, pH 7.2 (with KOH).

blocker mixture (Fig. 9*B*). We addressed whether the LVA calcium current contributed to this residual inward current by applying the T-type calcium channel blocker mibefradil at 2 μM (in the continuous presence of the HVA blocker mixture). These experiments were done either in external Tyrode's solution with 5 mM TEA-Cl ($n = 4$) or in 160 mM TEA-Cl solution ($n = 3$; both with 300 nM TTX). In six of seven cells there was a small current blocked by the addition of mibefradil (Fig. 10), active mainly during the repolarizing phase of the action potential. This mibefradil-sensitive current was always much smaller than either the TTX-R or the HVA calcium current, contributing −0.07 to −0.97 pC/pF (mean, −0.30 ± 0.31 pC/pF). This is consistent with previous observations of relatively small T-type currents in type 1 and type 2 DRG neurons (Cardenas et al., 1995). Even after mibefradil addition, a small (less than −50 pA peak amplitude) net inward current occasionally remained. This most likely represents a small fraction of HVA calcium current that remains unblocked by L-type, N-type, and P/Q-type channel blockers, as observed previously in some DRG neurons (Mintz et al., 1992). Such current may be carried by calcium channels formed by α1E subunits (Saegusa et al., 2000; Wilson et al., 2000).

Contribution of the inward currents to the action potential in small DRG cells

In 13 cells we were able to complete a series of solution changes to isolate each of the three predominant current types, i.e., TTX-S sodium current, TTX-R sodium current, and the HVA calcium current, and thus directly compare their relative amplitudes during the action potential. Figure 10 shows an example. In this cell, which was typical, the depolarizing current during the upstroke was contributed mainly by the TTX-R sodium current. TTX-S sodium current was much smaller (~20% at peak), but it activated earlier so that TTX-R and TTX-S currents were similar during the approach to threshold. HVA calcium current activated much more slowly than either TTX-S or TTX-R sodium currents and reached a peak during the shoulder of the action potential. Although the TTX-R sodium current reached a peak during the upstroke of the action potential, it was comparable in size to the HVA calcium current at the time of the shoulder. The LVA calcium current was much smaller than the HVA calcium current but did not have a dramatically different time course, reaching a peak during the shoulder.

To quantify the overall contribution of each type of current during the action potential, we integrated the current flowing during action potential clamp, measuring the total amount of charge transferred via that conductance. Each value was normalized to the cell capacitance. Figure 11 shows the charge carried by each current type for each cell in which a complete series of solution changes could be applied. In the vast majority of cells the TTX-R sodium conductance carried most of the overall inward charge during the action potential, with a moderate contribution

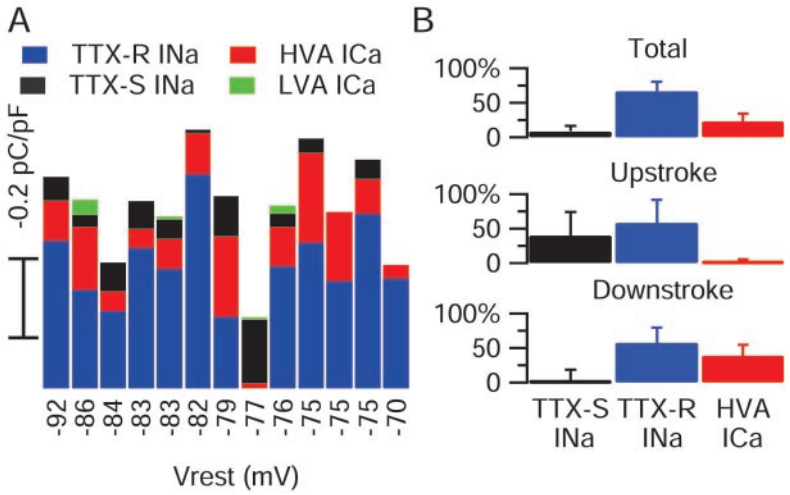

Figure 11. Contributions of the major inward currents to small DRG cell action potentials. *A*, The relative amplitudes of overall charge transferred by each conductance, recorded in the same cell, are plotted against the resting potential of the cell. An anomalous cell expressing purely TTX-S current is obvious (−77 mV resting potential). The latencies of the particular action potentials used for this analysis varied from 1.1 to 11.8 msec in different cells, and there was no significant difference in action potential parameters when action potentials were elicited in the same cell with different latencies in this range. *B*, Average normalized charge contributions by the TTX-S sodium, TTX-R sodium, and the HVA calcium current are shown for the overall duration of the action potential and separately for current flowing during the upstroke and downstroke. Error bars indicate SD.

by the HVA calcium conductance and relatively little contribution from either the TTX-S sodium current or the LVA calcium current. (One exception is the previously mentioned anomalous cell, probably not a nociceptor, that had a narrow action potential and expressed a purely TTX-S sodium current, visible as the largest TTX-S sodium charge in the graph.) In Figure 11 each cell is arranged by its resting potential. It is clear that the small contribution of TTX-S sodium current is not just a result of steady-state inactivation at the resting potential, because all but one cell had resting potentials of −75 mV or more negative, where the TTX-S current should be >50% available. Rather, these cells simply do not express high levels of TTX-S current. Overall, in the 12 likely nociceptors the TTX-R sodium current contributed 67 ± 14% of the total charge during the action potential, the TTX-S sodium current 9 ± 8%, and the HVA calcium current 23 ± 11% (n = 12).

The contribution of each current to either the upstroke or the downstroke of the action potential was analyzed by integrating the charge over a smaller time window. The currents during the upstroke were integrated from the initial depolarization until the action potential reached its maximum rate of depolarization, which occurred at +14 ± 5 mV. In this case, the TTX-R and TTX-S sodium currents were the largest contributors to the overall charge that was transferred, with a much smaller contribution of HVA calcium current. On average, the TTX-R sodium current supplied 58 ± 33% of the upstroke current, TTX-S sodium current 40 ± 34%, and HVA calcium current 2 ± 4% (n = 12).

To analyze inward currents contributing to the shoulder of the action potential, we integrated currents during the downstroke from the point at which the action potential reached +15 mV after the peak (approximately the beginning of the shoulder inflection) until a time when the inward currents had become zero (generally 10–15 msec later) (Figs. 1*A*, 7*A*). TTX-R sodium current supplied the greatest amount of total inward current during the downstroke (58 ± 22% of the total; n = 12), and HVA calcium channels also carried substantial current (39 ± 16%). TTX-S sodium current was negligible during this period (3 ± 17%), consistent with its nearly complete inactivation at the time of the peak.

DISCUSSION

These results show that TTX-R sodium current, TTX-S sodium current, and calcium currents all have different time courses during the action potential of nociceptor cell bodies. Both quantitatively and qualitatively, TTX-R sodium current plays the dominant role in that it carries the most total charge and flows at all stages of the action potential, from the approach to threshold to the shoulder on the falling phase.

The TTX-R sodium current we recorded presumably is formed by the expression of $Na_V1.8$ and $Na_V1.9$ channels. Judging from the activation and inactivation kinetics of the TTX-R current, it appears likely that $Na_V1.8$ channels carry the great majority of the current. The TTX-R current we measured inactivated nearly completely with voltage steps past −30 mV and inactivated with a time constant of ~5 msec at 0 mV, very similar to heterologously expressed cloned $Na_V1.8$ channels (Akopian et al., 1996; Vijayaragavan et al., 2001). The presumptive $Na_V1.9$-mediated current in neurons from $Na_V1.8$-null mice inactivates much more slowly (Cummins et al., 1999; but see Tate et al., 1998). The reason that $Na_V1.9$-mediated current seems to be small or absent in our recordings is not clear, because $Na_V1.9$ protein is present in the majority of nociceptors (Fang et al., 2002). However, we note that our recordings used different internal solutions (K-Mes-, TEA-Cl-, or NMDG-aspartate-based solutions in different experiments) than previous recordings of $Na_V1.9$-mediated current that used CsF-based internal solutions (Cummins et al., 1999). The $Na_V1.9$-mediated current is subject to slow inactivation at depolarized holding potentials, but this is unlikely to explain its absence in our recordings because the resting potentials in our experiments were, if anything, more negative (mean, −76 mV) than those generally reported for nociceptors. In fact, steady current through $Na_V1.9$ channels has been proposed to contribute to the more depolarized resting potentials sometimes seen in nociceptors (Herzog et al., 2001), consistent with such current being negligible in our recordings.

Although TTX-S sodium current carries somewhat less charge than TTX-R sodium current during the upstroke of the action potential, it activates more quickly and at smaller depolarizations so that both types of sodium current are likely to be important in setting the firing threshold of a cell. The inflammatory agent prostaglandin E_2, which sensitizes nociceptors and causes hyperalgesia, shifts the activation of the TTX-R sodium current to more hyperpolarized potentials and speeds activation kinetics at a given voltage (England et al., 1996; Gold et al., 1996). This would be expected to enhance the contribution of TTX-R current at voltages near threshold, which is already significant under basal

conditions. Consistent with this, prostaglandin E_2 and serotonin, which also enhances TTX-R current (Cardenas et al., 1997), both decrease the current threshold for excitation of nociceptors (England et al., 1996; Cardenas et al., 2001).

The contribution of TTX-S sodium currents to threshold and upstroke of nociceptor action potentials is likely to be sensitive to small changes in resting potential, because the midpoint of inactivation for TTX-S current is near −70 mV, and reported resting potentials of nociceptors range from −50 to −80 mV (Cardenas et al., 1995; Safronov et al., 1996; Petruska et al., 2000; Sung et al., 2000). However, even in neurons with resting potentials negative to −80 mV, where there is little steady-state inactivation of TTX-S current (Fig. 3), it still carried less charge than TTX-R current during the upstroke of the action potential (Fig. 11). Under conditions in which nociceptors have more depolarized resting potentials, the contribution of TTX-S sodium current would be even less, consistent with previous studies showing a minimal change on the current threshold after TTX application in a population of small DRG cells with an average resting potential near −50 mV (Caffrey et al., 1992). TTX-S sodium channels do provide substantial current to generate action potentials in small DRG cells from $Na_V1.8$ knock-out animals, perhaps because of compensatory upregulation (Renganathan et al., 2001).

It is striking that the TTX-R sodium current does not inactivate completely during the action potential, although action potentials in nociceptors are unusually broad. The slowness and incompleteness of TTX-R sodium current inactivation during the action potential helps to explain both the positive peaks (mean, +42 mV) and the long durations (mean half-maximal width of 4.7 msec) of the action potentials. The very positive peak suggests that the overall conductance is dominated by the sodium conductance at that point, and this conductance is overwhelmingly from TTX-R channels, because the TTX-S conductance is ~80% inactivated by the time of the peak (Fig. 8). The positive peak of the action potential is likely to be functionally significant in helping to maximize HVA calcium current activation.

In addition to inactivating incompletely during an action potential, TTX-R sodium current recovered quickly from inactivation after the action potential, much faster than TTX-S sodium current (Elliott and Elliott, 1993; Rush et al., 1998). In principle, the rapid recovery of TTX-R sodium current from fast inactivation (Fig. 8) could help to enable high firing rates (Elliott and Elliott, 1993; Schild and Kunze, 1997). However, the TTX-R sodium current in our recordings shows strong use dependence, declining in amplitude when stimulated at even modest rates of 1 Hz (cf. Rush et al., 1998). This reduction is apparently attributable to unusually prominent slow inactivation (also seen in cloned $Na_V1.8$ channels; Vijayaragavan et al., 2001) from which recovery is slow. Thus, although fast inactivation of TTX-R current is incomplete and recovers very quickly, slow inactivation of TTX-R sodium channels may limit the ability of cells to fire action potentials at a rapid rate.

Although HVA calcium currents carry substantial inward current during the shoulder of the action potential, TTX-R sodium current is even larger. In addition, the calcium current most likely activates a counterbalancing calcium-activated potassium current during the action potential shoulder. In contrast, Na entry through TTX-R sodium channels probably does not activate a potassium current; although Na-activated potassium currents are known to exist in small DRG neurons, they do not appear to be activated during single action potentials (Bischoff et al., 1998). The shoulder of the action potential in small DRG neurons has been found previously to be reduced or abolished completely by the application of inorganic divalent ions such as Cd^{2+} and Co^{2+} (Yoshida et al., 1978; Villiere and McLachlan, 1996; Abdulla and Smith, 1997). This is consistent with a significant contribution of calcium current, but Cd^{2+} and Co^{2+} also produce a partial block of TTX-R sodium current (Ikeda and Schofield, 1987; Roy and Narahashi, 1992), which may contribute to their effect.

We speculate that the functional significance of wide action potentials with prominent shoulders is related to the control of spike-elicited calcium entry. If this shape is characteristic of action potentials in the nerve terminals of nociceptors as well as cell bodies, it would produce large and long-duration presynaptic calcium transients (McCobb and Beam, 1991; Toth and Miller, 1995). The influence of TTX-R sodium current in shaping the action potential probably is not limited to the cell body, because there is evidence that TTX-R current contributes to the generation of action potentials in nerve endings of nociceptors (Brock et al., 1998; Strassman and Raymond, 1999) as well as the propagation of action potentials in unmyelinated C-fibers under some conditions (Jeftinija, 1994; Quasthoff et al., 1995). In addition, immunocytochemistry suggests that $Na_V1.8$ and 1.9 channels are expressed widely in unmyelinated DRG neurons, with labeling in peripheral endings, axons, somata, and nerve terminals (Amaya et al., 2000; Coward et al., 2000; Fjell et al., 2000; Fang et al., 2002).

The role of TTX-R sodium current in generating a shoulder on the action potential may be especially significant because it provides a mechanism by which the duration and amplitude of the shoulder can be varied independently of calcium currents. Calcium entry is likely to be very sensitive to changes in the shape of the shoulder (Toth and Miller, 1995; Wheeler et al., 1996), because a longer duration leads to more complete activation and slower deactivation, both very sensitive to voltage. Changes in calcium entry will, in turn, affect the shape of the shoulder in a complicated manner influenced by the extent of the activation of the calcium-activated potassium current. In contrast to calcium current, the TTX-R current during the shoulder is unlikely to be very sensitive to changes in the shape of the shoulder, because the channels have fully activated and partially inactivated by the time of the shoulder; if anything, a more prominent shoulder might decrease the TTX-R current by producing more complete inactivation. Because both TTX-R sodium channels and calcium channels can be modulated by various transmitters, the amount of calcium entry during the action potential could be controlled by directly modulating calcium channels or by modifying TTX-R current and thus changing the shape of the shoulder. Most transmitters that affect calcium current produce an inhibitory effect, whereas current through TTX-R channels is enhanced by prostaglandin E_2 and serotonin, hyperalgesic agents (England et al., 1996; Gold et al., 1996, 1998). Thus, enhancement of TTX-R current could enhance calcium entry by enhancing the shoulder of the action potential.

REFERENCES

Abdulla FA, Smith PA (1997) Ectopic α2-adrenoceptors couple to N-type Ca^{2+} channels in axotomized rat sensory neurons. J Neurosci 17:1633–1641.

Akopian AN, Sivilotti L, Wood JN (1996) A tetrodotoxin-resistant voltage-gated sodium channel expressed by sensory neurons. Nature 379:257–262.

Akopian AN, Souslova V, England S, Okuse K, Ogata N, Ure J, Smith A, Kerr BJ, McMahon SB, Boyce S, Hill R, Stanfa LC, Dickenson AH,

Wood JN (1999) The tetrodotoxin-resistant sodium channel SNS has a specialized function in pain pathways. Nat Neurosci 2:541–548.
Amaya F, Decosterd I, Samad TA, Plumpton C, Tate S, Mannion RJ, Costigan M, Woolf CJ (2000) Diversity of expression of the sensory neuron-specific TTX-resistant voltage-gated sodium ion channels SNS and SNS2. Mol Cell Neurosci 15:331–342.
Bischoff U, Vogel W, Safronov BV (1998) Na^+-activated K^+ channels in small dorsal root ganglion neurons of rat. J Physiol (Lond) 510:743–754.
Brock JA, McLachlan EM, Belmonte C (1998) Tetrodotoxin-resistant impulses in single nociceptor nerve terminals in guinea-pig cornea. J Physiol (Lond) 512:211–217.
Caffrey JM, Eng DL, Black JA, Waxman SG, Kocsis JD (1992) Three types of sodium channels in adult rat dorsal root ganglion neurons. Brain Res 592:283–297.
Cardenas CG, Del Mar LP, Scroggs RS (1995) Variation in serotonergic inhibition of calcium channel currents in four types of rat sensory neurons differentiated by membrane properties. J Neurophysiol 74:1870–1879.
Cardenas CG, Del Mar LP, Cooper BY, Scroggs RS (1997) $5HT_4$ receptors couple positively to tetrodotoxin-insensitive sodium channels in a subpopulation of capsaicin-sensitive rat sensory neurons. J Neurosci 17:7181–7189.
Cardenas LM, Cardenas CG, Scroggs RS (2001) 5HT increases excitability of nociceptor-like rat dorsal root ganglion neurons via cAMP-coupled TTX-resistant Na^+ channels. J Neurophysiol 86:241–248.
Coward K, Plumpton C, Facer P, Birch R, Carlstedt T, Tate S, Bountra C, Anand P (2000) Immunolocalization of SNS/PN3 and NaN/SNS2 sodium channels in human pain states. Pain 85:41–50.
Cummins TR, Dib-Hajj SD, Black JA, Akopian AN, Wood JN, Waxman SG (1999) A novel persistent tetrodotoxin-resistant sodium current in SNS-null and wild-type small primary sensory neurons. J Neurosci 19:RC43(1–6).
d'Alcantara P, Cardenas LM, Swillens S, Scroggs RS (2002) Reduced transition between open and inactivated states underlies 5HT increased I_{Na} in rat nociceptors. Biophys J 83:5–21.
de Haas V, Vogel W (1989) Sodium and potassium currents recorded during an action potential. Eur Biophys J 17:49–51.
Dib-Hajj SD, Tyrrell L, Black JA, Waxman SG (1998) NaN, a novel voltage-gated Na channel, is expressed preferentially in peripheral sensory neurons and down-regulated after axotomy. Proc Natl Acad Sci USA 95:8963–8968.
Dichter MA, Fischbach GD (1977) The action potential of chick dorsal root ganglion neurones maintained in cell culture. J Physiol (Lond) 267:281–298.
Djouhri L, Bleazard L, Lawson SN (1998) Association of somatic action potential shape with sensory receptive properties in guinea-pig dorsal root ganglion neurones. J Physiol (Lond) 513:857–872.
Doerr T, Denger R, Trautwein W (1989) Calcium currents in single SA nodal cells of the rabbit heart studied with action potential clamp. Pflügers Arch 413:599–603.
Elliott AA, Elliott JR (1993) Characterization of TTX-sensitive and TTX-resistant sodium currents in small cells from adult rat dorsal root ganglia. J Physiol (Lond) 463:39–56.
England S, Bevan S, Docherty RJ (1996) PGE_2 modulates the tetrodotoxin-resistant sodium current in neonatal rat dorsal root ganglion neurones via the cyclic AMP-protein kinase A cascade. J Physiol (Lond) 495:429–440.
Fang X, Djouhri L, Black JA, Dib-Hajj SD, Waxman SG, Lawson SN (2002) The presence and role of the tetrodotoxin-resistant sodium channel $Na_V1.9$ (NaN) in nociceptive primary afferent neurons. J Neurosci 22:7425–7433.
Fjell J, Hjelmstrom P, Hormuzdiar W, Milenkovic M, Aglieco F, Tyrrell L, Dib-Hajj S, Waxman SG, Black JA (2000) Localization of the tetrodotoxin-resistant sodium channel NaN in nociceptors. NeuroReport 11:199–202.
Gallego R (1983) The ionic basis of action potentials in petrosal ganglion cells of the cat. J Physiol (Lond) 342:591–602.
Gold MS, Reichling DB, Shuster MJ, Levine JD (1996) Hyperalgesic agents increase a tetrodotoxin-resistant Na^+ current in nociceptors. Proc Natl Acad Sci USA 93:1108–1112.
Gold MS, Levine JD, Correa AM (1998) Modulation of TTX-R I_{Na} by PKC and PKA and their role in PGE_2-induced sensitization of rat sensory neurons *in vitro*. J Neurosci 18:10345–10355.
Harper AA, Lawson SN (1985) Electrical properties of rat dorsal root ganglion neurones with different peripheral nerve conduction velocities. J Physiol (Lond) 359:47–63.
Herzog RI, Cummins TR, Waxman SG (2001) Persistent TTX-resistant Na^+ current affects resting potential and response to depolarization in simulated spinal sensory neurons. J Neurophysiol 86:1351–1364.
Hodgkin AL, Huxley AF (1952) A quantitative description of membrane current and its application to conduction and excitation in nerve. J Physiol (Lond) 117:500–544.
Ikeda SR, Schofield GG (1987) Tetrodotoxin-resistant sodium current of rat nodose neurones: monovalent cation selectivity and divalent cation block. J Physiol (Lond) 389:255–270.
Jeftinija S (1994) The role of tetrodotoxin-resistant sodium channels of small primary afferent fibers. Brain Res 639:125–134.
Kostyuk PG, Veselovsky NS, Tsyndrenko AY (1981) Ionic currents in the somatic membrane of rat dorsal root ganglion neurons. I. Sodium currents. Neuroscience 6:2423–2430.
Llinás R, Sugimori M, Simon SM (1982) Transmission by presynaptic spike-like depolarization in the squid giant synapse. Proc Natl Acad Sci USA 79:2415–2419.
Lopez de Armentia M, Cabanes C, Belmonte C (2000) Electrophysiological properties of identified trigeminal ganglion neurons innervating the cornea of the mouse. Neuroscience 101:1109–1115.
Magistretti J, Mantegazza M, Guatteo E, Wanke E (1996) Action potentials recorded with patch-clamp amplifiers: are they genuine? Trends Neurosci 19:530–534.
Magistretti J, Mantegazza M, de Curtis M, Wanke E (1998) Modalities of distortion of physiological voltage signals by patch-clamp amplifiers: a modeling study. Biophys J 74:831–842.
McCleskey EW, Gold MS (1999) Ion channels of nociception. Annu Rev Physiol 61:835–856.
McCobb DP, Beam KG (1991) Action potential waveform voltage-clamp commands reveal striking differences in calcium entry via low and high voltage-activated calcium channels. Neuron 7:119–127.
Mintz IM, Adams ME, Bean BP (1992) P-type calcium channels in rat central and peripheral neurons. Neuron 9:85–95.
Neher E (1992) Correction for liquid junction potentials in patch-clamp experiments. In: Methods in enzymology, ion channels (Iverson LE, Rudy B, eds), pp 123–131. San Diego: Academic.
Ogata N, Tatebayashi H (1993) Kinetic analysis of two types of Na^+ channels in rat dorsal root ganglia. J Physiol (Lond) 466:9–37.
Park D, Dunlap K (1998) Dynamic regulation of calcium influx by G-proteins, action potential waveform, and neuronal firing frequency. J Neurosci 18:6757–6766.
Petruska JC, Napaporn J, Johnson RD, Gu JG, Cooper BY (2000) Subclassified acutely dissociated cells of rat DRG: histochemistry and patterns of capsaicin-, proton-, and ATP-activated currents. J Neurophysiol 84:2365–2379.
Porreca F, Lai J, Bian D, Wegert S, Ossipov MH, Eglen RM, Kassotakis L, Novakovic S, Rabert DK, Sangameswaran L, Hunter JC (1999) A comparison of the potential role of the tetrodotoxin-insensitive sodium channels, PN3/SNS and NaN/SNS2, in rat models of chronic pain. Proc Natl Acad Sci USA 96:7640–7644.
Quasthoff S, Grosskreutz J, Schroder JM, Schneider U, Grafe P (1995) Calcium potentials and tetrodotoxin-resistant sodium potentials in unmyelinated C fibres of biopsied human sural nerve. Neuroscience 69:955–965.
Ransom BR, Holz RW (1977) Ionic determinants of excitability in cultured mouse dorsal root ganglion and spinal cord cells. Brain Res 136:445–453.
Renganathan M, Cummins TR, Waxman SG (2001) Contribution of $Na_V1.8$ sodium channels to action potential electrogenesis in DRG neurons. J Neurophysiol 86:629–640.
Ritter AM, Mendell LM (1992) Somal membrane properties of physiologically identified sensory neurons in the rat: effects of nerve growth factor. J Neurophysiol 68:2033–2041.
Roy ML, Narahashi T (1992) Differential properties of tetrodotoxin-sensitive and tetrodotoxin-resistant sodium channels in rat dorsal root ganglion neurons. J Neurosci 12:2104–2111.
Rush AM, Brau ME, Elliott AA, Elliott JR (1998) Electrophysiological properties of sodium current subtypes in small cells from adult rat dorsal root ganglia. J Physiol (Lond) 511:771–789.
Saegusa H, Kurihara T, Zong S, Minowa O, Kazuno A, Han W, Matsuda Y, Yamanaka H, Osanai M, Noda T, Tanabe T (2000) Altered pain responses in mice lacking α1E subunit of the voltage-dependent Ca^{2+} channel. Proc Natl Acad Sci USA 97:6132–6137.
Safronov BV, Bischoff U, Vogel W (1996) Single voltage-gated K^+ channels and their functions in small dorsal root ganglion neurones of rat. J Physiol (Lond) 493:393–408.
Schild JH, Kunze DL (1997) Experimental and modeling study of Na^+ current heterogeneity in rat nodose neurons and its impact on neuronal discharge. J Neurophysiol 78:3198–3209.
Scroggs RS, Fox AP (1992a) Calcium current variation between acutely isolated adult rat dorsal root ganglion neurons of different size. J Physiol (Lond) 445:639–658.
Scroggs RS, Fox AP (1992b) Multiple Ca^{2+} currents elicited by action potential waveforms in acutely isolated adult rat dorsal root ganglion neurons. J Neurosci 12:1789–1801.
Strassman AM, Raymond SA (1999) Electrophysiological evidence for tetrodotoxin-resistant sodium channels in slowly conducting dural sensory fibers. J Neurophysiol 81:413–424.
Sung KW, Kirby M, McDonald MP, Lovinger DM, Delpire E (2000) Abnormal $GABA_A$ receptor-mediated currents in dorsal root ganglion neurons isolated from Na-K-2Cl cotransporter null mice. J Neurosci 20:7531–7538.
Swandulla D, Armstrong CM (1989) Calcium channel block by cadmium in chicken sensory neurons. Proc Natl Acad Sci USA 86:1736–1740.

Taddese A, Bean BP (2002) Subthreshold sodium current from rapidly inactivating sodium channels drives spontaneous firing of tuberomammillary neurons. Neuron 33:587–600.

Tate S, Benn S, Hick C, Trezise D, John V, Mannion RJ, Costigan M, Plumpton C, Grose D, Gladwell Z, Kendall G, Dale K, Bountra C, Woolf CJ (1998) Two sodium channels contribute to the TTX-R sodium current in primary sensory neurons. Nat Neurosci 1:653–655.

Toth PT, Miller RJ (1995) Calcium and sodium currents evoked by action potential waveforms in rat sympathetic neurones. J Physiol (Lond) 485:43–57.

Vijayaragavan K, O'Leary ME, Chahine M (2001) Gating properties of $Na_V1.7$ and $Na_V1.8$ peripheral nerve sodium channels. J Neurosci 21:7909–7918.

Villiere V, McLachlan EM (1996) Electrophysiological properties of neurons in intact rat dorsal root ganglia classified by conduction velocity and action potential duration. J Neurophysiol 76:1924–1941.

Waxman SG, Cummins TR, Dib-Hajj S, Fjell J, Black JA (1999) Sodium channels, excitability of primary sensory neurons, and the molecular basis of pain. Muscle Nerve 22:1177–1187.

Wheeler DB, Randall A, Tsien RW (1996) Changes in action potential duration alter reliance of excitatory synaptic transmission on multiple types of Ca^{2+} channels in rat hippocampus. J Neurosci 16:2226–2237.

Wilson SM, Toth PT, Oh SB, Gillard SE, Volsen S, Ren D, Philipson LH, Lee EC, Fletcher CF, Tessarollo L, Copeland NG, Jenkins NA, Miller RJ (2000) The status of voltage-dependent calcium channels in α1E knock-out mice. J Neurosci 20:8566–8571.

Yoshida S, Matsuda Y, Samejima A (1978) Tetrodotoxin-resistant sodium and calcium components of action potentials in dorsal root ganglion cells of the adult mouse. J Neurophysiol 41:1096–1106.

Zhou W, Jones SW (1995) Surface charge and calcium channel saturation in bullfrog sympathetic neurons. J Gen Physiol 105:441–462.